DETERMINATION AND IMPROVEMENT OF SPATIAL RESOLUTION FOR DIGITAL ARIAL IMAGES

S. Becker [a], N. Haala [a], R. Reulke [b]

[a] University of Stuttgart, Institute for Photogrammetry, Germany
[b] Humboldt-University, Dept. Computer Science, Computer Vision, Germany
Susanne.Becker@ifp.uni-stuttgart.de

KEY WORDS: geometry, calibration, high resolution, spatial, performance

ABSTRACT:

Triggered by the spread of digital aerial image acquisition, the quantification and improvement of spatial image resolution has become a topic of considerable interest for photogrammetric processing. Within our paper, the determination of image resolution based on the Rayleigh criterion and the point spread function will be discussed. These techniques then can be applied in order to exactly evaluate the quality of approaches aiming on the enhancement of image resolution. In our investigations such a resolution improvement is realised based on a linear restoring finite impulse response filter. This type of algorithm is especially suitable, if images from different camera modules are available. This will be demonstrated exemplarily using image data captured from so-called staggered arrays, which are for example available in the digital aerial camera ADS40. The improvement of spatial resolution is also applied in the context of pan-sharpening algorithms, which combine multispectral imagery with higher resolution panchromatic data. This will be demonstrated in the final part of the paper.

1. INTRODUCTION

The quantification and improvement of image resolution has been a topic of considerable interest within the remote sensing community for more than 20 years. Due to the availability of digital airborne cameras, these techniques are meanwhile also used within photogrammetric applications. In order to quantify the spatial resolution of spaceborne or airborne data, frequently the ground sampling distance (GSD) of the image is determined. This parameter is defined by pixel distance in the camera's focal plane projected to the ground. For this reason, the GSD can be computed easily for images captured from digital airborne cameras. Nevertheless, if the images to be evaluated are transformed geometrically before photogrammetric processing, the determinability of this parameter is limited. Such geometric pre-processing is frequently applied for high-end digital airborne cameras since these systems realise a large field of view and a high geometric resolution either by a multi-component or a pushbroom approach. As an example, systems like the ZI/Imaging DMC (Hinz, 2000) and the Vexcel Ultracam (Leberl, 2003) integrate several component images to one large full-frame image, while pushbroom cameras like the Leica ADS40 (Sandau, 2000) scan the terrain surface with CCD-line sensors in order to collect large image strips at large swath widths. Both approaches require a geometric transformation during pre-processing in order to generate 'virtual' images prior to further photogrammetric evaluation. Within the multi-head approach, the original images as they are provided from single staring arrays are stitched together resulting in one large image, which is used for further processing. In the case of pushbroom cameras, geometric pre-processing comprises the rectification of the original image strips to a reference surface in order to remove image distortions due to aircraft movement. These pre-processing steps during generation of the virtual images can hinder the direct link of their spatial resolution to the respective parameters of the digital camera. In order to measure the spatial resolution of such virtual images, the size of the smallest details that can be identified by an operator in an image can be determined, alternatively. Nevertheless, since this parameter depends on an operator-based interpretation, this type of values can be subjective.

For these reasons, our paper addresses an approach aiming on an objective and simple measurement of spatial resolution for digital airborne images. As it will be discussed in section 2.1, this resolution concept applies the definition of Rayleigh, which is based on the differentiation of structures. According to this definition, the resolution limit of a system is equivalent to the angular distance of two point sources, which just can be distinguished. The advantage of this approach is, that distances in the object space can be directly linked to properties of the camera system. By these means also the improvement of image resolution, which can be obtained by the use of dedicated filters and algorithms, can be quantified. Such an improvement of spatial resolution by suitable post processing steps is frequently aspired in order to support the evaluation and interpretation of the imagery by a human operator. Section 2.2 discusses an approach, which allows the effective improvement of image resolution based on image restoration. The algorithm to be used within our work is the linear restoring finite impulse response (FIR) filter, which estimates the original grey value for each pixel position from the surrounding image values. The estimated optimal restoration of the original scene increases the contrast and sharpness especially for smaller structures and thus enhances the visibility of details.

The applicability of the algorithms for determination and improvement of spatial resolution will be demonstrated for two application scenarios in section 3. The first example deals with the staggered array approach. It is a method that merges two panchromatic data sets in order to get an increased sampling rate and an improved spatial resolution. The enhancement of spatial resolution by the use of staggered arrays will be exemplarily demonstrated for the digital aerial camera ADS40, where two parallel CCD lines are shifted against each other by half a pixel.

For almost all digital aerial cameras, the spatial resolution of the multispectral images is smaller compared to the panchromatic data. Nevertheless, multispectral data at the resolution of the

panchromatic images can be generated, if a suitable pan-sharpening algorithm combines the imagery. This technique is used for satellite images since many years, thus several approaches are available. As it will be demonstrated within section 4, these techniques can also be applied for airborne images. Based on our approach, the improvement of resolution can be determined, objectively. Additionally, the quality of the pan-sharpening algorithms with respect to the achieved preservation of colour values will be discussed, briefly.

2. RESOLUTION IMPROVEMENT BY IMAGE RESTORATION

Beside additive noise, image resolution is mainly limited by blur, which is influenced by factors like the atmosphere, relative motion of the depicted object, defocusing of the optics, or the finite size of the aperture and the detector (Reulke, 2004). As it will be discussed in the following section, this blur can be described and measured efficiently using the point spread function (PSF). Based on this theory, in section 2.2 an approach aiming on the improvement of image resolution by reconstructing the original image from its degraded version is described.

2.1 Measurement of image degradation

Blurring occurs in any imaging system that uses electromagnetic radiation. The most common degradations are caused by imperfections of the sensors or by transmission. With respect to the optics, defocusing and the limited spatial extent of the aperture, lenses and mirrors are the main reasons for image degradation. Scattering of light between the target object and the imaging system as well as motion of the object or the system during data collection introduce additional image deterioration. A further effect resulting in blurring is given by the discretisation since the CCD detectors average illumination over regions. Generally, the blur of the system is characterized by the PSF or impulse response.

Thus, the resolution of an imaging system can be described in terms of the PSF of the system. Since the PSF can be measured easily at image edges, which are either provided from a test pattern like a Siemens star or from natural structures, the objective and simple quantification of image resolution is feasible. A convenient approach is the analysis of radial modulation of the Siemens star (see Figure 1).

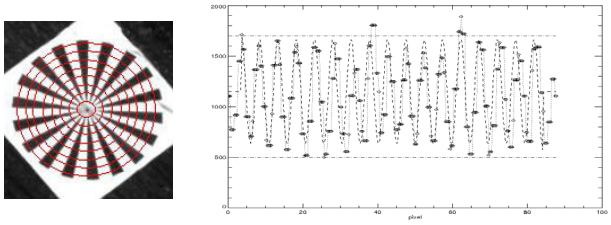

Figure 1. Radial modulation analysis for one circle of the Siemens star

The diameter of the star is proportional to the circumference of a circle and can be analysed in relation to image pixel size. As it can be seen in the left part of Figure 1, grey values are measured along circles. The right part of Figure 1 presents the measured grey values for one circle exemplarily. Different diameters realise variable spatial frequencies. The evaluation of the modulation for different radii gives a quantitative prediction for the resolution. After computing the modulation M for each frequency (see equation (1)), the modular transfer function (MTF) can be derived.

$$M = \frac{I_{max} - I_{min}}{I_{max} + I_{min}} \tag{1}$$

with I_{max} - maximal and I_{min} - minimal grey value.

The resulting MTF can be modelled with a Gaussian shape function (Jahn, 1995). Thus, its shape is specified by σ_{MTF}. Equation (2) shows the MTF in the one-dimensional case.

$$MTF \cong e^{-2\pi^2\sigma_{MTF}^2 K^2} \tag{2}$$

The connection between the σ_{MTF} of the MTF and the σ_{PSF} of the corresponding PSF is given by the following inverse proportional relationship

$$\sigma_{PSF} = \frac{1}{2\pi\sigma_{MTF}} \tag{3}$$

By means of the σ_{PSF}, it is possible to compare different camera systems or imaging conditions. Additionally, the improvement of image resolution can be quantified.

2.2 Image restoration

Image restoration, which aims on resolution improvement by reconstructing the original image from its degraded version, is an ill-posed inverse problem. For this reason, there is no unique solution, and a small amount of noise can result in large reconstruction errors. Thus, it is necessary to have some a priori knowledge on the original scene and PSF as well as noise information. There are several approaches, which apply different degrees of a priori knowledge. The method we use within this paper is the linear restoring finite impulse response (FIR) filter. The estimation of the scene values $\hat{I}_{i,j}(x,y)$ from the actually measured intensities $I'_{i,j}(x,y)$ is based on following formula (Reulke, 2003):

$$\hat{I}_{i,j} = \sum_{k,l} a_{k,l} \cdot I'_{i-k,j-l} \tag{4}$$

For the determination of the optimal filter coefficients $a_{k,l}$ a least mean square solution is used. The FIR filter approach is a local algorithm that assumes the noise to be zero-mean and white. The original scene $I(x,y)$ is expected to be a stationary random process that contains the information for stabilisation of the reconstruction problem. This kind of a priori knowledge can be controlled with a regularisation parameter

$$\varepsilon^2 = \sigma_{noise}^2 / \kappa_{scene}^2 \tag{5}$$

Thus, in order to determine the parameter ε, a priori information on the noise σ_{noise} and the original scene κ_{scene} is required. The influence of different ε-values on the process of image restoration is demonstrated in Figure 2. While large ε-values lead to a smoothing effect, as it can be seen for ε = 0.5, small ε-values result in a visible resolution improvement but also in increasing noise (see the examples for ε = 0.07 and ε = 0.03). The optimal values for ε and σ_{noise} can be extracted from the maximum of the figure of merit (FOM) presented in Figure 3. Since the FOM is given by the product of the σ_{MTF} and the signal-to-noise ratio, it represents a system performance metric that includes both resolution and sensitivity measures. In all following calculations σ_{noise} =0.8 pixel and ε=0.07 are used as optimal restoration parameters, which allow for a considerable improvement of image resolution at an acceptable decrease of the signal-to-noise-ratio.

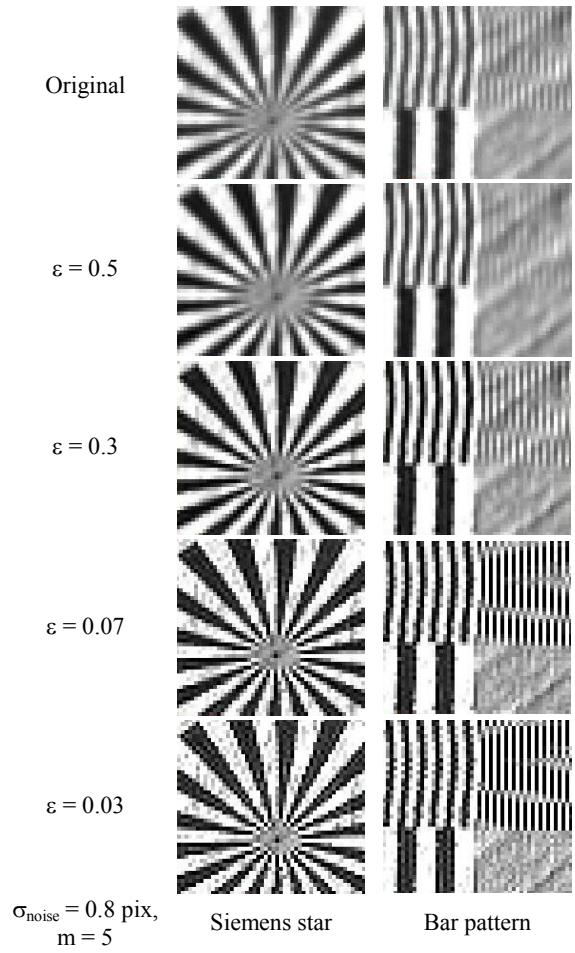

Figure 2. Result of restoration algorithm for σ_{noise} = 0.8 pixel and different ε-values (with m = filter size)

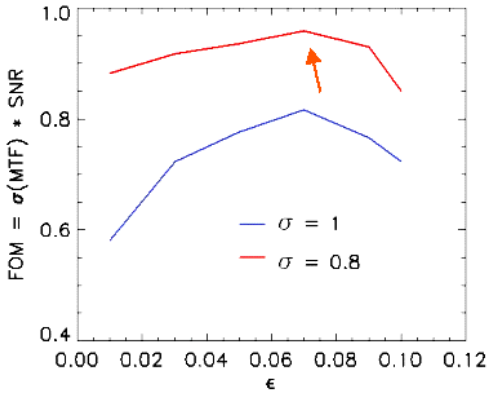

Figure 3. Resolution and SNR as a function of the ε-value

3. RESOLUTION IMPROVEMENT BY STAGGERED ARRAYS

One goal of our work on resolution determination and improvement was to take advantage of the so-called staggered array configuration, which is realised within the airborne pushbroom camera ADS40. Usually, such sensors feature a focal plane with three panchromatic CCD lines capturing panchromatic information in forward, nadir and backward view. Additionally, the ADS40 sensor opts for using staggered line arrays for resolution improvement. Thus, each panchromatic channel exhibits two parallel 12k CCD lines shifted against each other by half a pixel (Sandau, 2000).

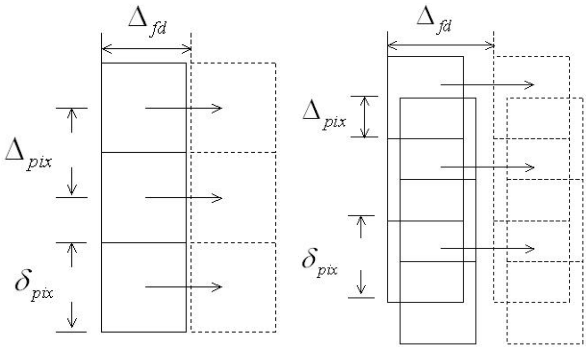

Figure 4. Sampling for linear and staggered CCD lines

As it is depicted in Figure 4, for a single line array the sampling distance in line direction Δ_{pix} is equal to the detector size δ_{pix}. The sampling limit or the Nyquist frequency is $1/(2\delta_{pix})$. In the case of staggered arrays the sampling distance is reduced to half of the pixel size, which results in the doubled Nyquist frequency $1/\delta_{pix}$ (Holst, 1998).

3.1 Data collection and pre-processing

If aerial pushbroom imagery is applied, image distortions resulting from aircraft motion have to be eliminated by a suitable preprocessing step prior to photogrammetric evaluation. For this purpose, the image is geometrically rectified by projecting each pixel in the image space on a reference plane at the mean terrain height. Within this process, the respective orientation and position of the original scan line is applied.

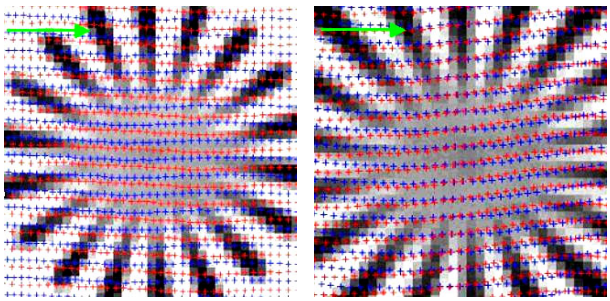

Figure 5. Optimal and sub-optimal sampling pattern

This process is exemplarily demonstrated in Figure 5. The blue crosses refer to pixels captured by the first, while red crosses refer to pixels captured by the second CCD line of the staggered array configuration. As it is indicated by the green arrow, the direction of flight is from left to right. After the geometric transformation, the mapped image pixels are irregularly distributed on the reference plane. At each of these points the grey value of the corresponding original image pixel is available. For further processing these grey values are interpolated to a regular image grid by a Natural Neighbours interpolation (Sibson, 1981). By these means, the grey value images in the background of Figure 5 were generated.

3.2 Resolution determination

Figure 6 shows the result of such an interpolation, which was generated from a single CCD line (left) and two staggered lines (right).

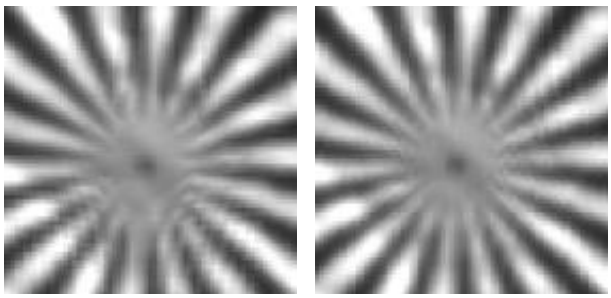

Figure 6. Examples of not staggered (left) and staggered (right) images

As it is demonstrated within this figure, due to the extended cut off frequency, the staggered array approach allows for reconstructing even higher frequent signals correctly. Aliasing effects can be suppressed and the quality of staggered images is improved. Within the left image of Figure 6, considerable aliasing effects in the middle of the Siemens star are clearly visible. In contrast, these effects are reduced in the staggered image.

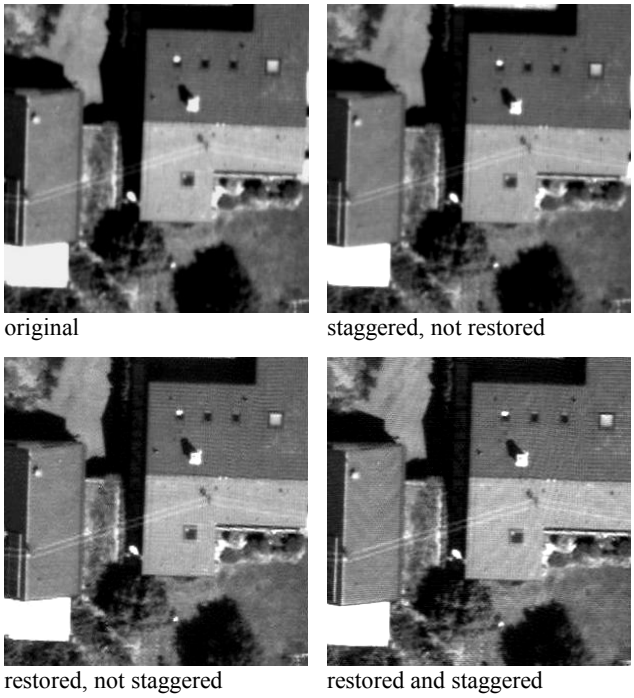

original | staggered, not restored

restored, not staggered | restored and staggered

Figure 7. Result of staggering and image restoration

In addition to an enhanced quality, the staggered array results in an improved spatial resolution of the image. However, this resolution enhancement strongly depends on the respective sampling pattern. In the ideal case, as it is depicted in Figure 4, the sampled points of the staggered lines form a regular grid on the ground. Nevertheless, flight motions during image collection can prevent this optimal sampling pattern, as it is visible for the real data presented in Figure 5. While the left image, which was captured at a flying height of 4000m shows a nearly optimal sampling pattern, the sampled points of the right image, which was captured at a flying height of 2500m are distributed quite unfavourably. This directly affects the resolution improvement that is determined by the evaluation of the corresponding MTF. With an optimal sampling pattern a spatial resolution enhancement of about 15% was measured, while for a sub-optimal pattern this number reduces to a value of only 8%. Figure 7 gives some additional results on the impact on data collection by staggered arrays in combination with image restoration for a natural scene. Compared to the original data set the restored and not staggered image seems to be sharper. Additionally, small structures like the tiles appear more clearly. If the restoration is based on staggered data, the image resolution is additionally increased to some degree.

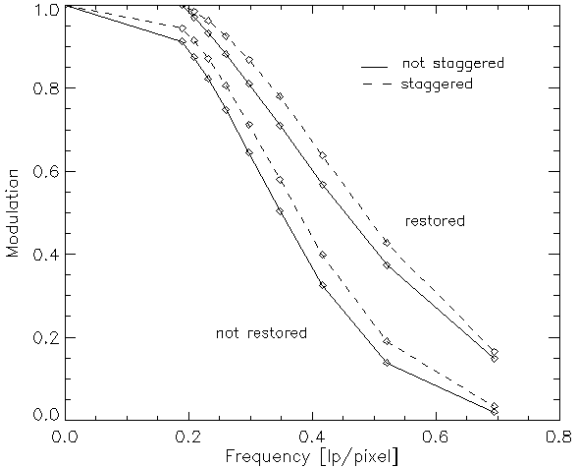

Figure 8. MTF of restored and/or staggered image data

These effects could be quantified by images of a Siemens star, which were captured and processed in the same configuration as in Figure 7. The MTF that belong to these data sets are presented in Figure 8. They are derived using equation (1) from the radial modulation analysis for different circles of the Siemens star as depicted in Figure 1.

	σ_{PSF} [pixel]	
	not staggered	staggered
not restored	0.51	0.47
restored	0.39	0.36

Table 1. σ_{PSF} of restored and/or staggered image data

Table 1 contains the σ-values of the corresponding PSF (see equation (3). By means of image restoration the spatial resolution can be improved of about 24%. With both image restoration and staggering a resolution improvement can be achieved of 30%.

4. PAN-SHARPENING

In contrast to panchromatic data multispectral images generally feature a smaller spatial resolution. To overcome this drawback a variety of pan-sharpening algorithms have already been developed. Comparable to the staggered array approach, the idea of the pan-sharpening consists in merging different data sets. In this case, multispectral images are combined with panchromatic data of higher resolution. According to their design, these methods can be grouped in different classes as for example the substitution methods, the arithmetic and the filter based techniques. In this section some pan-sharpening methods and evaluation criteria will be introduced and validated, subsequently.

Substitution methods rely on replacing the structural component of the multispectral image with the panchromatic image data (Bretschneider, 2000). Prior to this substitution, the structural information of the multispectral data must be extracted. Well-known approaches based on the substitution method are the IHS (Intensity, Hue, Saturation) - and HSV (Hue, Saturation,

Value) - transformation and the PCA (Principal Components Analysis) (Zhang, 2002; Gonzalez, 1992). The principle of the arithmetic methods consists in merging panchromatic and multispectral grey values by means of arithmetic operations like addition, subtraction, multiplication and division (Pohl, 1998). One member of this class of algorithms is given by the Brovey transformation (Vrabel, 1996). The concept of the filter-based techniques is to eliminate the spatial structures from the panchromatic image with the help of filters and add them to the multispectral data (Gonzalez, 1992). Depending on the filter characteristics various approaches can be distinguished. Of considerable interest is a high-pass filter (HPF) that is based on an image restoration algorithm, the FIR filter.

4.1 Colour preservation

The objective of all pan-sharpening algorithms is the resolution improvement of multispectral images while retaining the original colour values. As before, determining the MTF and the PSF, respectively, can do the quantification of the resolution improvement. In order to analyse the colour preservation, the grey values of the multispectral images before and after the pan-sharpening should be compared. For this purpose it is important to find an appropriate colour space. A great disadvantage of the RGB-model is, that the subjective perception of colour differences depends on the colour itself. Therefore, a comparison of RGB-values does not reflect the perceptual colour impression. In this respect the CIE-L*a*b* colour space seems to be more dedicated (Bunting, 1998; Franke, 1997).

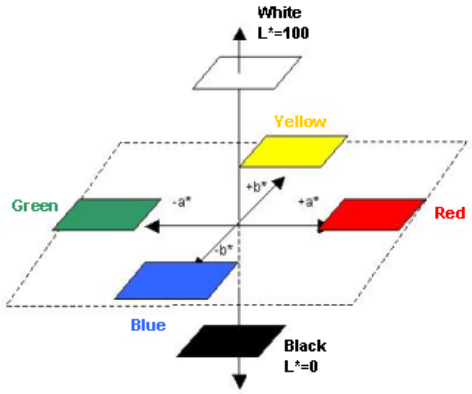

Figure 9. CIE-L*a*b* colour space

As it is shown in Figure 9 every colour is described by an intensity component L and two hue values a and b. Unlike the RGB-model, geometrical distances in the L*a*b*-space correspond to approximate the same perceptual colour differences. Thus, all following investigations of colour values are carried out in the L*a*b*-model. If the L*a*b*-distance between two colours is lower than 2, a colour difference can hardly ever be observed, whereas strong colour deviations result in colour distances greater than 5 (Hartl, 2004). First of all, the preservation of the colour values was examined. Initial results showed noticeable colour deviations throughout all approaches, confirmed by colour distances all greater than 5. A refinement of this quite poor result can be reached, if a histogram matching is applied before the pan-sharpening. By a linear scaling (equation (6)) the histogram of the panchromatic image P is first adapted to the histogram of the intensity image I, which can be derived from the multispectral data.

$$P^{old} = m \cdot P^{new} + d \qquad (6)$$

$$\text{with } m = \frac{I_{max} - I_{min}}{P^{old}_{max} - P^{old}_{min}} \text{ and } d = \frac{P^{old}_{max} \cdot I_{min} - P^{old}_{min} \cdot I_{max}}{P^{old}_{max} - P^{old}_{min}}.$$

In doing so, the measured colour distances range between 2.4 and 3.9. So the remaining colour differences are reduced to a tolerable degree.

Figure 10. Original multispectral image

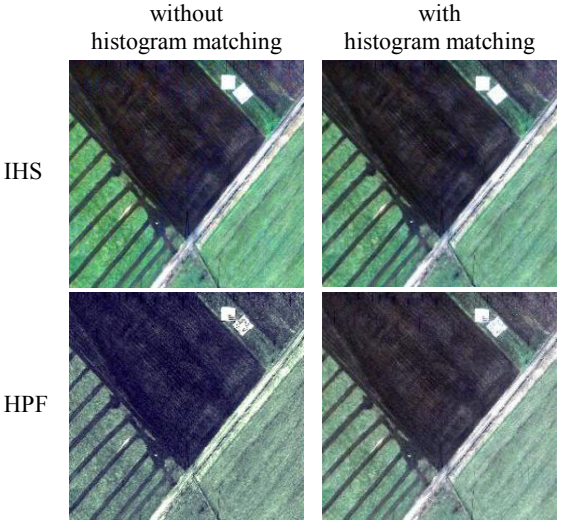

Figure 11. Pan-sharpening results with and without histogram matching

While Figure 10 shows the original multispectral image, Figure 11 presents the pan-sharpening results with and without an a priori histogram matching exemplarily for the IHS- and the HPF-methods. The corresponding mean colour distances ΔE are listed in Table 2.

	ΔE			
	IHS	PCA	Brovey	HPF
without histogram match.	8.8	12.7	8.7	8.3
with histogram match.	2.4	2.7	2.4	3.9

Table 2. Colour distances ΔE in the CIE-L*a*b*-space

4.2 Resolution improvement

In order to have a visible effect of resolution improvement, we choose multispectral data with a sampling distance in flight direction that is twice as large as the one in line direction, whereas the corresponding panchromatic image has the same sampling distance in both directions. Figure 12 shows the multispectral image (σ_{PSF} =1.4 pixel) to be much more blurred than the panchromatic image (σ_{PSF} =0.63 pixel). As indicated by the yellow arrow, the flight direction in this example is from top to bottom.

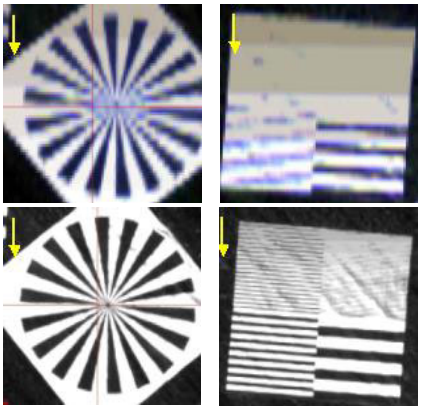

Figure 12. Multispectral and panchromatic input data

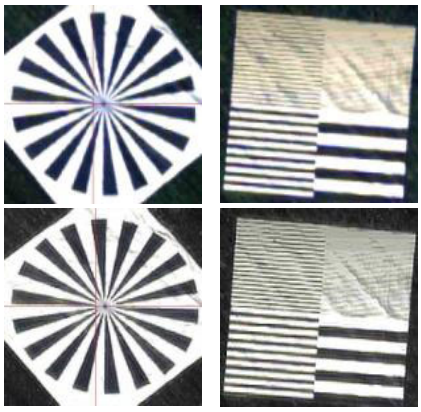

Figure 13. Pan-sharpening results

As it is depicted in Figure 13, by applying the IHS-algorithm the resulting multispectral images feature with a σ_{PSF} of 0.64 pixel almost the same spatial resolution as the panchromatic data that exhibits a σ_{PSF} of 0.63 pixel. Similar results are obtained by the PCA- and the Brovey algorithm. If the HPF-approach is applied, the resulting spatial resolution of 0.42 pixel is even better than the resolution of the panchromatic input. This considerable resolution improvement can be attributed to the influence of the underlying FIR filter.

5. CONCLUSIONS

Within the paper, a framework for resolution analysis was presented. By these means, the advantages of image restoration algorithms to fully exploit the potential of digital airborne image collection are demonstrated. While the determination of image resolution is an important issue for analysing the quality of pre-processed data, resolution improvement is especially important, if data from multiple camera modules has to be integrated.

REFERENCES

Bretschneider, T., Kao, O., 2000. Image Fusion in Remote Sensing. Proceedings of the 1st Online Symposium of Electronic Engineers.

Bunting, F., 1998. The ColorShop Color Primer. Light Source Computer Images, Inc. An X-Rite Company.

Franke, K.-H., 1997. Grundlagen der Farbbildverarbeitung. Skript zur Vorlesung. Technische Universität Ilmenau.

Gonzalez, R.C., Woods, R.E., 1992. *Digital Image Processing*. Reading, Mass.: Addison-Wesley.

Hartl, S., 2004. http://www.copyshop-tips.de/luf07.php (accessed March 2004).

Hinz, A., 2000. Digital Modular Camera: System Concept and Data Processing Workflow. *The International Archives of the Photogrammetry, Remote Sensing and Spatial Information Sciences*. Amsterdam, Vol. 33, Part B2, pp. 164.

Holst, G.C., 1998. *Sampling, Aliasing and Data Fidelity for Electronic Imaging Systems, Communications, and Data Acquisition*. SPIE, Bellingham.

Jahn, H., Reulke, R., 1995. *Systemtheoretische Grundlagen optoelektronischer Sensoren*. Akademie Verlag, Berlin.

Leberl, F., 2003. The UltraCam Large Format Aerial Digital Camera System. Proceedings of the ASPRS Annual Convention. Anchorage / Alaska, USA, May 5-9 (CD only).

Pohl, C., van Genderen, J.L., 1998. Multisensor Image Fusion in Remote Sensing: Concepts, Methods and Applications. *International Journal of Remote Sensing*, Vol. 19, No. 5, pp. 823-854.

Reulke, R., 2003. Bildverarbeitung und Mustererkennung II. Skript zur Vorlesung. Universität Stuttgart, WS 02/03.

Reulke, R. et al., 2004. Improvement of Spatial Resolution with Staggered Arrays as used in the Airborne Optical Sensor ADS40. Commission I, WG I/4.

Sandau, R., 2000. Design Principles of the LH Systems ADS40 Airborne Digital Sensor. *The International Archives of the Photogrammetry, Remote Sensing and Spatial Information Sciences*. Amsterdam, Vol. 33, Part B2, pp. 552-559.

Sibson, R., 1981. *A brief Description of Natural Neighbour Interpolation*. V. Barnet, (ed) Interpreting Multivariate Data. John Wiley & Sons, pp. 21-36.

Vrabel, J., 1996. Multispectral Imagery Band Sharpening Study. *Photogrammetric Engineering and Remote Sensing*, Vol. 62, No. 9, pp. 1075-1083.

Zhang, Y., 2002. Problems in the Fusion of Commercial High-Resolution Satellite Images as well as Landsat 7 Images and Initial Solutions. *International Archives of Photogrammetry and Remote Sensing*, Vol. 34, Part 4.